



# ATLAS NOTE

August 18, 2017



## Performance of a Micromegas Trigger Processor with Cosmic Ray Muons

N. Felt<sup>a</sup>, M. Franklin<sup>a</sup>, P. Giromini<sup>a</sup>, J. Philion<sup>a</sup>, C. Rogan<sup>a</sup>, A. Tuna<sup>a</sup>, A. Wang<sup>a</sup>

<sup>a</sup>*Harvard University, Cambridge, Massachusetts 02138, USA*

### Abstract

We built a strong, beautiful, and brave Micromegas octuplet, and we instrumented it with MMFE8 front-end boards, ART Data-Driver Cards, and a Trigger Processor. The trigger performance for  $\geq 0.8 \text{ GeV}/c^2$  cosmic muons is described.

# 1 Introduction

We investigate the performance of the micromegas Address in Real Time (ART) and trigger processor. This is one of the two trigger technologies introduced for the New Small Wheel (NSW) upgrade of the ATLAS muon spectrometer, which is intended to be built and installed in the coming years.

The performance is measured with hundreds of thousands of cosmic muons recorded at the Harvard cosmic ray test stand, which employs a full trigger electronics path with prototype hardware: MMFE8s equipped with VMM2, the FPGA-based ADDC V1, and a micromegas trigger processor (MMTP) implemented on a VC707 FPGA evaluation board.

This note presents the performance of the trigger data path; the full readout data path is described in previous notes [4, 5] using the same detectors and similar electronics. The reader is encouraged to read these notes for complementary measurements and a better understanding of the performance of the micromegas detectors and electronics in a broader context.

## 2 Experiment

The micromegas and scintillator detectors of the Harvard cosmic ray test stand are described in detail in previous notes presenting the performance of the full MMFE8 readout [4, 5]. Eight layers of micromegas detectors are stacked vertically for the purpose of providing eight measurements of the position of a cosmic muon as it travels through the experiment. The readout strips of each layer have a pitch of 0.4 mm, and they are arranged as designed for the NSW: XXUVUVXX, where strips in the  $X$  planes run perpendicular to the readout edge of the chamber, and strips in the  $U$  ( $V$ ) planes are tilted at an angle of  $1.5^\circ$  ( $-1.5^\circ$ ) to provide a measurement of the non-precision coordinate. Each layer of micromegas is 20 cm by 20 cm.

Three layers of scintillators with PMTs for light detection are placed above, on top of, and below the micromegas to provide a trigger for the full MMFE8 readout. A scintillator trigger is formed when all three layers of scintillator detect a coincidence. There is  $\sim 2 - 3$  meters of concrete between the micromegas and the bottom scintillator to filter low-energy particles.

### 2.1 Electronics

The micromegas readout paths in this note include three cards. The MMFE8 is the front-end readout card, and it houses 8 VMM2 ASICs per card. These readout chips receive signals from the detector and digitize them, and they are discussed in great detail elsewhere [1, 4, 5]. The MMFE8 also houses an FPGA for configuring and reading out the VMMs over ethernet. The experiment in this note has 8 layers of micromegas detectors and therefore 8 MMFE8s.

The ART Data Driver Card (ADDC) is a driver card for the micromegas trigger data path. It receives data from 4 MMFE8s over mini-SAS connections and packages this data into a single output for downstream clients. The card houses an FPGA for this purpose. There are 2 ADDCs in this experiment to receive data from the 8 MMFE8s.

The Micromegas Trigger Process (MMTP) is the last card of the micromegas trigger path. It receives data from ADDCs over fiber optical connections and interrogates the data for the presence of triggers. The card houses an FPGA for this purpose. There is 1 MMTP in this experiment to receive data from the 2 ADDCs. An ADDC V1 and a prototype MMTP are shown in Figure 1.

Additionally, a board was built at Harvard for the purpose of operating the MMFE8s synchronously, referred to as the clock/trigger board. This board sends a 40 MHz clock to all 8 boards, which are used by each board as a mother clock, thereby synchronizing them. The board also receives trigger signals from

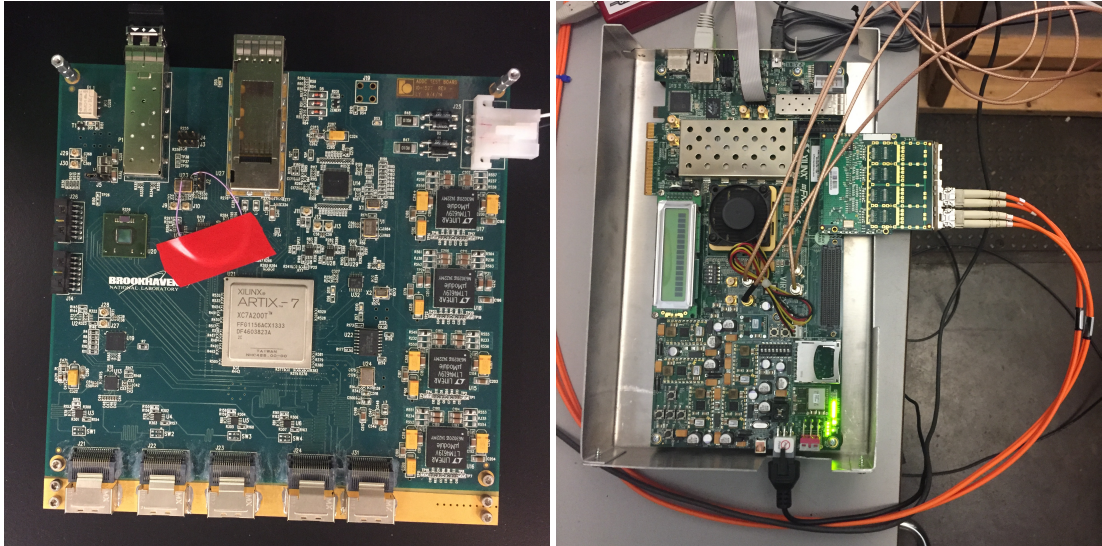


Figure 1: An FPGA-based ADDC V1 on the bench (left) and the MMTP placed on a VC707 FPGA evaluation board (right) in the laboratory.

the scintillator and distributes them to the MMFE8s, as discussed in Section 2.3. A cartoon schematic of the electronics is shown in Figure 2.

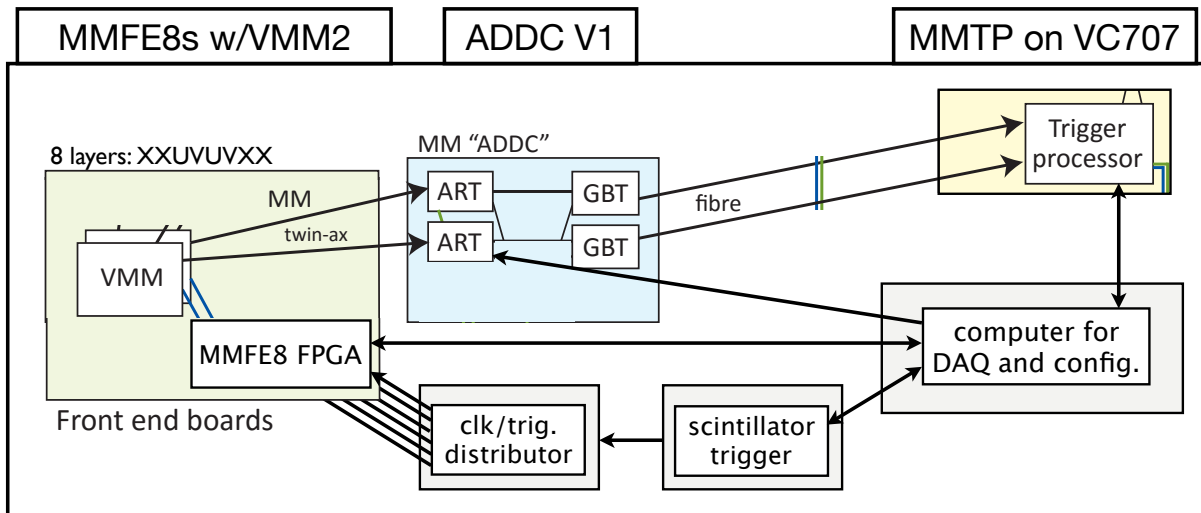


Figure 2: Cartoon schematic of the data flow in the electronics used at the Harvard cosmic ray test stand. Inspiration for the cartoon is provided by L. Levinson.

## 2.2 Trigger data path

The micromegas trigger data path begins at the VMM. The data path is referred to as the Address in Real Time (ART) data path, which refers to the output of the VMM. The full readout can include many strips per BC, and each strip read out includes lots of information about the strip, including charge (PDO) and time (BCID, TDO). Alternatively, the trigger readout sends the data from at most one strip per BC, and it only includes the address of the strip. This is the crux of the trigger data path; the bandwidth of the trigger data path is greatly reduced relative to the full readout. One bit is used to announce a hit is

recorded, and six bits are used for the address.

The VMM has two operating modes for the ART: at-threshold and at-peak. These modes describe the time at which an ART signal is sent by the VMM. Threshold mode is faster than peak mode because the VMM sends the signal as soon as a threshold is crossed, instead of waiting until a peak is found. The data in this note are taken with the ART operating at threshold.

The VMM sends ART data over mini-SAS cables to the ART Data-Driver Card (ADDc), which collects ART signals from 4 MMFE8 and packages them into a single output. The ART data bypasses the MMFE8 readout chip entirely. The data in this note are taken with ADDc V1, in which the ADDc has an on-board FPGA for collecting and packaging the incoming signals. The final version of the ADDc will have on-board ASICs for this purpose, since it will be mounted in the ATLAS cavern and must be radiation tolerant. However, the functionality of the FGPA-based and ASIC-based ADDc are expected to be identical.

The ADDc then sends the packaged ART data to the micromegas trigger processor (MMTP). The communication protocol is “GBT”, which was developed at CERN as a radiation hard bi-directional optical link for LHC upgrades. The signals are sent over fiber optic cables. The MMTP collects ART signals, analyzes them for patterns resembling a trigger, and sends trigger information to downstream clients. These steps are performed by an FPGA. The data in this note are taken with an implementation of the MMTP on a Xilinx VC707 development board with a Virtex-7 FPGA.

In this setup, 2 ADDcs are placed near the detector and accept ART signals from the 8 MMFE8s. The VC707 is placed further from the detector in a counting room, along with the DAQ computer and scintillator readout electronics. It accepts signals from both ADDcs.

### 2.3 MMFE8 and scintillator data path

The MMFE8 and scintillator data paths are described in detail elsewhere [4, 5]. In brief, the DAQ computer communicates directly with the MMFE8s over ethernet connection. The full MMFE8 readout includes charge and time information for each strip above threshold in the form of PDO, TDO, and BCID. The MMFE8 only sends data over ethernet after it has received a trigger signal from the scintillator. The signal is sent from the scintillator to the clock/trigger board over coaxial cable, and the clock/trigger board sends this signal to the 8 MMFE8s over microHDMI.

The scintillator trigger is formed with a coincidence of six signals corresponding to the top, middle, and bottom scintillator counters. The signals are acquired by Lecroy TDC and sent to a CAMAC crate controller, which then sends its data over ethernet to the DAQ computer.

### 2.4 Scintillator timestamp

Additionally, there is a connection between the scintillator electronics and the MMTP, to utilize the fast internal clocks of the MMTP FPGA. The scintillator trigger signal is sent directly to the MMTP, which captures the signal using a 640 MHz clock and forwards this timestamp to the DAQ computer over ethernet. This is referred to as the *scintillator timestamp*. It provides a more accurate reference time than the scintillator BCID captured by the MMFE8s, since the 640 MHz clock of the MMTP allows for  $\sim 1.56$  ns resolution, versus the  $\sim 25$  ns resolution of the 40 MHz clock.

## 3 MMTP Algorithm

The MMTP algorithm and performance is described in detail elsewhere [2, 3]. The algorithm is reviewed in brief here, and adjustments needed to operate the MMTP with a cosmic muon detector are highlighted.

The MMTP algorithm is designed to receive ART data from the ADDC, decode the data, group the data into subsets (“triggers”) which satisfy a spatial and temporal coincidence, and calculate quantities which describe these triggers. The first step is referred to as the *decoder*, the second step is referred to as the *finder*, and the third step is referred to as the *fitter*.

The MMTP algorithm is written in firmware and placed on a Xilinx Virtex-7 FPGA, which is housed by a VC707 evaluation board. The algorithm meets timing requirements for synthesis and implementation of the algorithm on the FPGA. Ultimately, the algorithm will be placed on a larger FPGA on a high-density optical mezzanine card (“HORX”) which will be housed in an ATCA shelf. The VC707 implementation is already capable of testing many aspects of the algorithm, however, including the steps mentioned above.

### 3.1 Decoding

ART data is transmitted from the ADDC to the MMTP using the GBT protocol via optical fibers. The data is transmitted as one 128-bit word per BC per ADDC. 12 bits describe the BCID; 32 bits describe which of the 32 VMMs associated with one ADDC are transmitting an ART signal; 48 bits give a maximum of 8 ART strip numbers, which are 6 bits each; and the remaining bits are used for checking data quality, such as an 8-bit data parity word.

After receiving the ART data, the MMTP converts the VMM and strip numbers into global strip numbers, also taking into consideration that some of the MM chambers are flipped relative to each other. For example, if an ART strip from VMM 5 is reported as strip number 30, the MMTP converts this to a global strip number of 350 ( $5 * 64 + 30$ ). The units of the MMTP are strip pitches, and there is no conversion to a unit of meters. The MMTP then adds the distance from the beamline to the base of the MM chamber, in units of strips, to the global strip number, and divides the global strip number by the  $z$ -position of the chamber, to convert the strip to a slope,  $x_{\text{strip}}/z_{\text{strip}}$ .

### 3.2 Finder

Once the ART data is received and decoded, the next step of the MMTP algorithm is to filter the data into subsets which roughly look like an incident particle traversing the octuplet. This step is called the *finder*.

The finder relies heavily on parallelization. A configurable number of roads are created in the FPGA to span the octuplet, and each road evaluates in parallel whether it contains a sufficient number of ART strips to form a trigger. In this note, the road size is 1 road per VMM. This is demonstrated graphically in Figure 3.

Additionally, the roads should overlap to avoid edge cases where the incident muon travels near the boundary of two roads. This is implemented in the finder by allowing each road to use hits not only in their respective road, but also in neighboring roads. The number of neighboring roads is a configurable parameter; in this note, hits from one neighbor above and one neighbor below are used in a given road. For example, road 3 uses hits from VMM 2, VMM 3, and VMM 4, so that the effective road size is 3 VMMs.

The effective road size is chosen as the smallest possible road size which accepts most or all of the cosmic muons passing through the detectors. The incident angle of cosmic muons is shown in previous studies with this detector [4, 5], which is at most 25 degrees. Muons with an angle of 26 degrees can be observed with an effective road size of 3 VMMs, as shown in Figure 4, though some inefficiency can be expected starting at 18 degrees, depending on the position of the muon.

A road must contain at least two hits on horizontal ( $X$ ) planes and at least two hits on stereo ( $UV$ ) planes to satisfy a trigger. Additionally, at least two of the hits on  $X$ -planes must occur on opposite quadruplets, to ensure a good lever arm when fitting the  $X$ -hits to a line. These requirements are looser

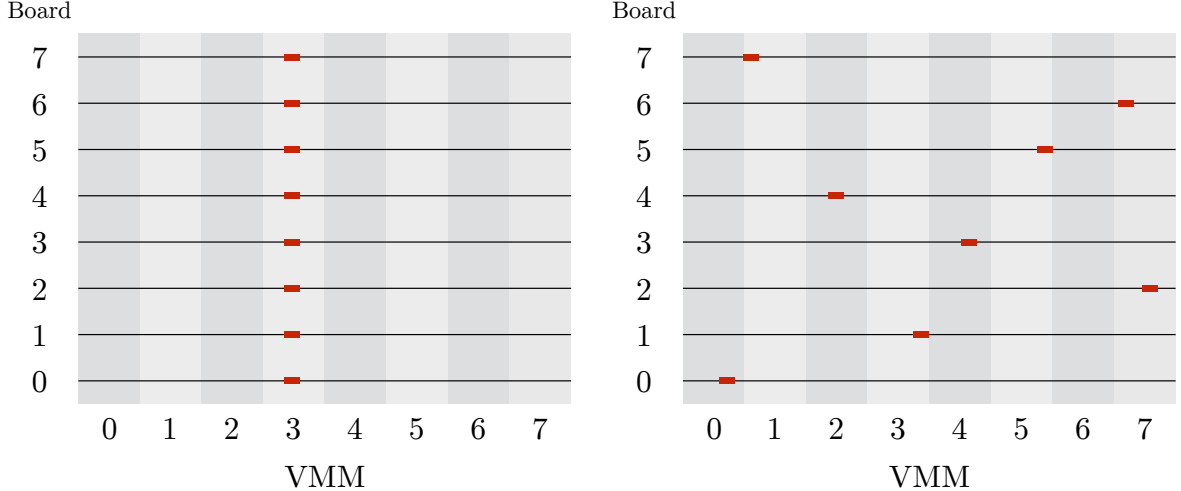


Figure 3: Cartoon demonstration of a collection of hits which look like a cosmic muon passing through the chamber (left) and a collection which looks random (right). Roads are 1-VMM wide and shown in alternating gray colors. Only the cartoon on the left would form a trigger.

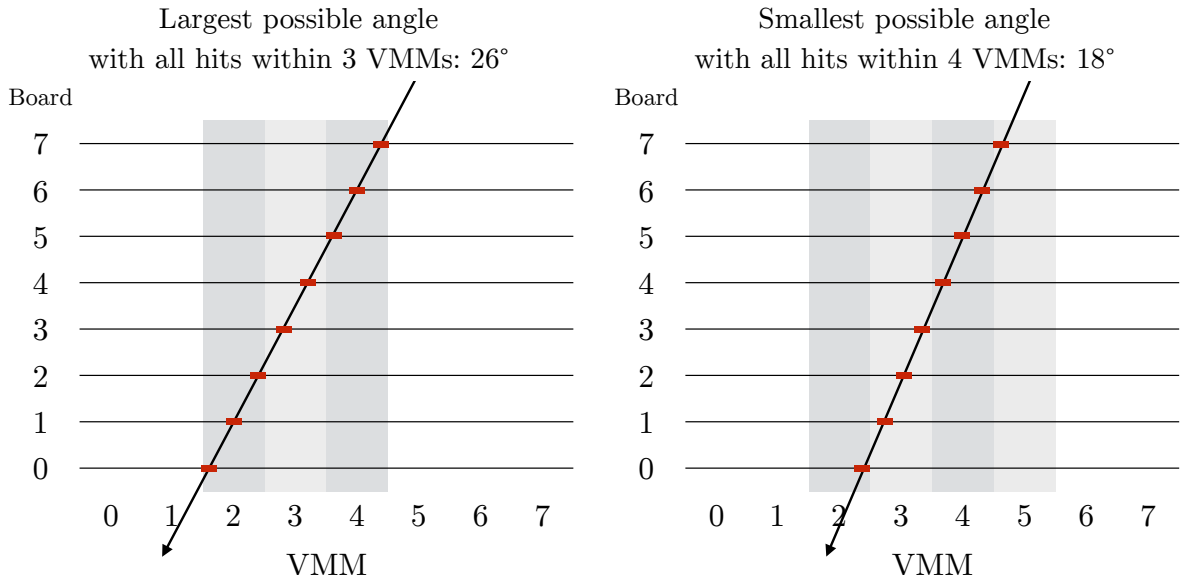


Figure 4: Cartoon demonstration of the highest-angle track with all 8 hits spread across 3 VMMs (left) and the lowest-angle track with at least one hit spread across 4 VMMs (right). The angles are 26 and 18 degrees, respectively. An effective road size of 3 VMMs should then have 100% hit efficiency up to 18 degrees.

than the expected coincidence requirements at the NSW (3X AND 3UV), since the rate of noise and background hits is much lower for cosmic data-taking than at the LHC.

The finder also requires hits for a trigger to be within a time window in units of the BC clock. The expected time window for the NSW is two BCs; in this note, the window is increased to seven BCs to maximize efficiency and measure the efficiency of the window as a function of the size of the window. The time window is implemented as follows. When a hit arrives at the finder, it is stored in memory for seven BCs. For each road satisfied by the hit, no new hits are allowed in that road for that board until

the hit is “old”, i.e., after seven BCs. As hits are recorded, the coincidence requirements are evaluated for all roads in parallel. Once the coincidence requirements for a road are met and the earliest hit in the road becomes “old”, a trigger is formed. Therefore hits are collected in a time window of seven BCs, and triggers cannot be formed until the oldest hit in the road is sufficiently old.

The stipulation that a hit in a road on a board cannot be overwritten by a new hit is motivated by the behavior of the detector and the ART data-flow: an incident muon is expected to leave a signal on multiple strips on a board (making a “cluster”), each strip of which can send an ART signal typically separated by a couple of BCs. Only the first hit from the cluster should be used for the trigger, hence the earlier hit should not be overwritten by subsequent nearby hits.

Every road is capable of forming one trigger per cycle of the BC clock. After evaluating all roads in parallel, the triggers created are placed in a priority encoder to be sent sequentially to the fitter for further calculations. The priority encoder sorts the triggers by road number, with smallest roads treated first. Because the MMTP clock is eight times faster than the BC clock, there can be at most eight triggers per BC.

### 3.3 Fitter

The triggers found by the finder are then sent to the *fitter*, which calculates quantities of interest for the trigger. The fitter presently does not create or remove any triggers. The final implementation of the MMTP algorithm may include a quality requirement from the fitter, namely  $\Delta\theta < 15^\circ$ .

For the NSW, the main deliverables of the fitter are the location and quality of a trigger. The location is represented by a region of interest (ROI), which is a number provided by downstream clients like Sector Logic mapping to  $\eta - \phi$  space. The quality of the trigger is represented by the difference in angle a *local* fit of the trigger ART hits and a *global* fit. A *local* fit is performed on only the ART hits, and a *global* fit is performed with the constraint that the trigger be consistent with the interaction point. The difference is called  $\Delta\theta$ .

The location of the trigger is derived in a Cartesian  $m_x - m_y$  space, where  $\hat{y}$  points perpendicular to the direction of the X-strips,  $\hat{x}$  points parallel to the X-strips, and  $m_i$  is the slope  $i/z$ .  $m_y$  is measured as the average of slopes measured in each X-plane,  $\bar{m}_X$ .  $m_x$  is measured as the difference between slopes measured in the *U* and *V* planes, with a geometric factor from the angle of the stereo strips:  $\frac{m_U - m_V}{2 \tan(\theta_{\text{stereo}})}$ . The standard ATLAS coordinates  $\eta, \phi$  can be derived directly from  $m_x, m_y$ , where the resolution of  $\eta (\phi)$  is dominated by the resolution of  $m_y (m_x)$ . Rather than calculate  $\eta, \phi$ , however, the slopes  $m_i$  are sent as an address to a LUT which returns a ROI.<sup>1</sup>

To calculate the quality of a trigger, the fitter compares the slopes of a linear fit of the ART data with and without a constraint that it originate at the interaction point. These are referred to as *global* and *local* slopes, respectively, and they only use hits from the X-planes. The global slope is simply the aforementioned  $m_y$ , or  $\bar{m}_X$ . The local slope is calculated as  $m_x^{\text{local}} = \sum c_i y_i$ , where the sum includes all X hits,  $c_i$  is a constant depending on which X-planes are used in the fit, and  $y_i$  is the position of the hit.  $c_i$  is stored in a LUT, and the multiplication/addition is performed by the FPGA. This analytic “fit” gives the slope of the least-squares line, and is more appealing than an iterative fit given the hardware constraints. The difference in angles  $\Delta\theta$  can be calculated directly from  $m_x^{\text{local}}, m_x^{\text{global}}$ , but instead these slopes are sent as an address to a LUT which returns  $\Delta\theta$ .

### 3.4 Output

The MMTP will send its triggers to the sTGC trigger processor FPGA, where duplicates will be discarded before being sent to downstream clients. The NSW TP in total will send at most 8 triggers per BC per

---

<sup>1</sup>We apologize for the confusing notation. To recap: *X*, *U*, and *V* denote different layers of micromegas. *x*, *y*, and *z* are cartesian coordinates. The *X*-layers measure  $m_X$ , which is used to derive  $m_y$ . And so on.

sector. Each trigger will be composed of 24 bits, and presently the bits are allocated as 5 bits for  $\Delta\theta$ ; 5 bits for  $\phi$  ROI; 8 bits for  $\theta$  ROI; and 6 spare bits.

### 3.5 Adjustments for cosmic muons

The use of *slopes* instead of *strips* in the algorithm is motivated by the knowledge that particles arriving at the NSW from a proton-proton collision should travel in a nearly straight line. Thus, each layer of MM will record a different strip address for the incident particle, but a nearly identical slope. This simplifies logic for defining spatial *slope-roads* in the MM chamber.

However, for a cosmic ray test stand, the exact origin of incident particles is unknown. The MMTP algorithm is then modified to use strip addresses instead of slopes for the definition of roads, as discussed in Section 3.2. The implementation of strip-to-slope conversion in the FPGA is nonetheless tested by multiplying each strip address by 1, instead of  $1/z_{\text{strip}}$ , to calculate a “slope” which is suitable for spatial coincidences of cosmic muons. Using strips instead of slopes is the largest conceptual difference between the ATLAS implementation and the cosmic muon implementation of the algorithm, and it will be relevant for the analysis in Section 5.

Additional adjustments to the MMTP algorithm for use at the cosmic ray test stand include:

- The overall chamber offset from the beamline is removed, though the machinery of adjusting the overall offset is kept
- Plane-specific offsets from the beamline are essentially removed, though the machinery of adjusting the global strip is kept
- The number of neighboring roads considered for each road in the finder is 2 for  $X$  and  $UV$  planes, whereas for ATLAS it is 2 (5) for  $X$  ( $UV$ )
- The constants  $c_i$  of the local slope calculation depend on the geometry of the octuplet, and are adjusted for the mini-octuplet
- Offline, the precision coordinate of the MMTP is referred to as  $x$ , and the non-precision coordinate is  $y$ , because we found it confusing otherwise.

Finally, the MMTP algorithm stores copies of the input ART data and output trigger data in FIFO buffers, which are transmitted as UDP packets via ethernet to a computer for analysis.

## 4 Data-taking

The data described in this note was taken from May 2017 until July 2017. Each continuous period of data-taking is referred to as a “run”, and the runs are described in Table 1.

The astute reader will notice there are many more MMTP events than MMFE events. There are three reasons for this. First, the MMTP sends data whenever the finder creates a trigger, whereas the MMFE only sends data when it receives a trigger signal from the scintillator. The MMTP then records many more triggers due to low energy cosmic muons, cosmic muons which miss the scintillators, and random noise which happens to satisfy the loosened trigger requirements. Run 3522 in particular observed more triggers from noise than the other runs. Second, the MMTP will typically make a handful of triggers for a single cosmic muon passing through the detector due to the overlapping roads. For example, a downward-going muon passing entirely through road 2 will make triggers in roads 1, 2, and 3. Third, if the incoming ART data is spread across many BCs, the MMTP will often make triggers on multiple BCs as the hits arrive.

These last two circumstances are an open issue of the firmware logic, and duplicates will likely need to be removed from the MMTP before being sent to the sTGC trigger processor. In this note, if many triggers are created by the MMTP to describe a single muon, the trigger with the most hits is chosen for analysis.

Between Runs 3522 and 3527, two front-end cards were repaired and replaced on the detector. Therefore the data from Run 3522 is presented as the default performance in Section 5, whereas the data from Runs 3527, 3528, and 3530 are used for comparing the performance for different integration times in Section 5.5

Run	Dates	MMFE Events	MMTP Events	Notes
3522	05/11 - 05/18	296532	15774567	200 ns integration time
3527	06/26 - 07/02	233645	3635093	100 ns integration time
3528	07/02 - 07/07	205053	3253330	50 ns integration time
3530	07/19 - 07/24	192114	4060891	200 ns integration time

Table 1: Information about each run of data-taking.

## 4.1 Combining data streams

Three data streams are produced by the MMTP and written to disk, in addition to the scintillator and MMFE data streams. Two of the MMTP streams are written when a trigger is found. First, the trigger itself is output, which includes a BCID of the trigger, the ART hits of the trigger, and the quantities describing the trigger which are produced by the fitter. Second, all of the incoming ART hits in a window of 15 BCs around the trigger are output. The BCIDs of the hits used by the trigger are extracted from the second stream, and it is additionally useful for debugging the behavior of the algorithm offline. The third stream is independent of the algorithm, and it writes a 16-bit BCID to disk whenever it receives a trigger from the scintillator. This stream runs on a 640 MHz clock and allows for offline comparison of the TP trigger BCID to the scintillator BCID in steps of 1.56 ns.

All streams are synchronized and combined offline by comparing the machine time of their respective DAQ scripts as they are written to disk. The second MMTP trigger stream is additionally required to contain all of the hits recorded in the first MMTP stream.

## 5 Performance

The performance of the ART and MMTP in this note is described relative to the full MMFE8 and scintillator readout, which is to say, the efficiency and resolution is not measured absolutely. For each cosmic muon event, the scintillator is required to have good data quality, and the full MMFE8 readout is required to record a track with at least two clusters in the X-planes on opposite quadruplets and at least two clusters in the stereo planes. Every event passing this criteria should create a trigger in the MMTP.

### 5.1 Basic performance

The MMTP shows excellent efficiency for finding a trigger given the criteria described above. Figure 5 shows the efficiency for finding a trigger as a function of time (left) and the number of hits in the trigger as a function of time (right). Both figures indicate stable performance throughout the run.

The triggers created by the MMTP are also in good agreement with the expectation from the full MMFE8 readout, as shown in Figure 5. The angular distribution (right) is nearly identical between the

MMTP and the MMFE8s, where the angle of the MMTP is the angle evaluated in the FPGA, and the angle of the MMFE8 track is the angle calculated offline. The hit multiplicity (left) is similar between the MMTP and the MMFE8s, though on average the MMTP records fewer hits per track. This is due to the 7 BC collection window discussed in Section 3.2. Occasionally, this window is still not large enough, and an ART hit arrives too late to be considered for the trigger. The collection window is also likely the cause of the sub-percent inefficiency observed in Figure 5.

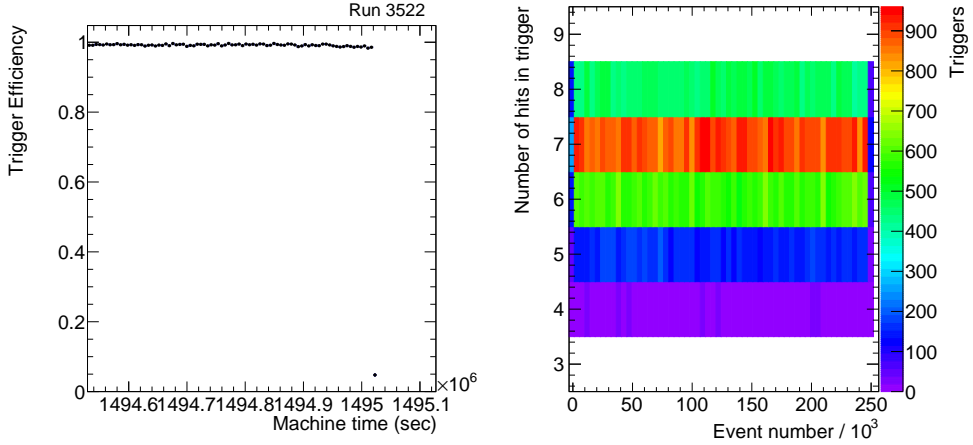


Figure 5: The efficiency of a trigger to be matched to a full readout event versus time (left) and the number of hits in the trigger as a function of time (right). Both figures show stable data-taking.

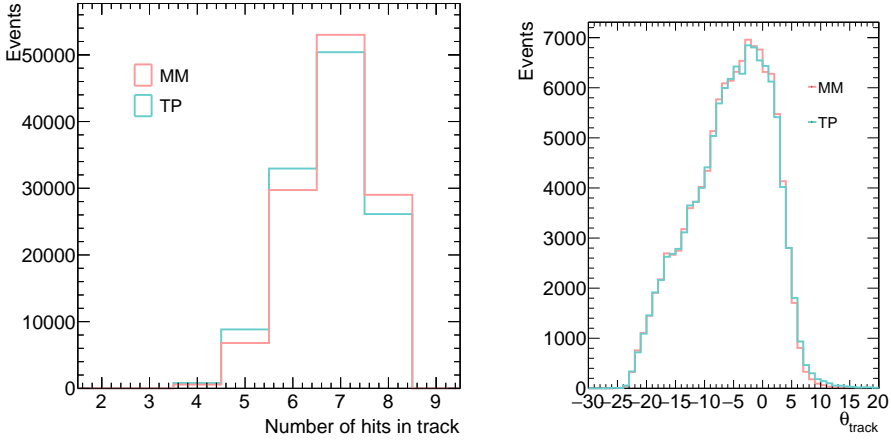


Figure 6: The number of hits in the MMTP and MM FE tracks (left) and the angle of the tracks (right). The track found by the trigger closely resembles the track found by the full readout, though with slightly fewer hits on average.

## 5.2 Offline roads

An additional trigger quality requirement is considered when measuring the resolution of the MMTP. As discussion in Section 3.2, the road size configured in the FPGA is 1 VMM, or effectively 3 VMMs when including neighboring roads. This allows muons with large incident angle to form triggers in the MMTP, but it is also vulnerable to background hits since the effective road is much larger than needed for a

downward-going muon. This vulnerability is less relevant for the NSW implementation of the algorithm because it will use *slope-roads*, which is equivalent to only triggering on downward-going muons when using simple, strip-based roads.

To avoid this vulnerability, the resolution measured is presented in two ways. First, the resolution measured by the MMTP is shown unadulterated. Second, the resolution is shown for triggers which satisfy *offline roads*, to emulate the slope-roads of the NSW implementation. Offline roads are defined relative to the reference track of the full MMFE8 readout. The position of this track is evaluated at each layer, and a road is created around this position. The offline roads in this note are defined as 16 strips (1/4 VMM), with neighbors on either side, which is approximately the size of the slope-roads suggested for the NSW. Therefore an ART hit on a given layer must be within 24 strips of the track to “satisfy” the road. A trigger is said to satisfy the offline road if all the hits of the trigger satisfy the road individually.

An important caveat is that even slope-roads cannot be simply defined for stereo planes. Unlike horizontal strips, the slope of a stereo strip measured at one edge of the wedge is different than the slope measured at the other edge. The MMTP defines the slope of a stereo strip as the slope evaluated in the center of the wedge, and as the road size is made smaller, it can become inefficient for tracks traversing the wedge near the edges. Therefore the road size for stereo planes must be larger than for horizontal planes.

In this note, the offline stereo road is made larger by approximately the amount which will be needed at the NSW. This amount is smallest in the region closest to the beamline of the SM1 chamber, and largest in the region farthest from the beamline of the LM2 chamber, as shown in Figure 7. This corresponds to 13 mm (or 33 strips) and 58 mm (or 144 strips), respectively. The two offline stereo roads in this note are then 1/4 VMM, with neighboring roads, plus either of these tolerances. Coincidentally, an offline road of 1/4 VMM with an extra 144 strips is 192 strips, or 3 VMMs, so no offline requirement is needed on top of the 1 VMM road required online by the FPGA.

### 5.3 Spatial and angular resolution

The spatial resolutions measured with cosmic data are shown in Figures 8 and 9. The  $x$  resolution is measured as the difference between the average  $x$  position of the trigger hits on the  $X$  planes and the  $x$  position of the fitted MMFE8 track evaluated at the average  $z$  position of the trigger hits. Calculating the average of trigger  $X$  hits corresponds directly to calculating the average of  $X$  slopes at the NSW, also known as  $m_X^{\text{global}}$ , which dominates the  $\eta$  measurement. The  $y$  resolution is measured as the difference between the difference of average  $x$  position of  $U$  and  $V$  planes, with the geometric factor  $\frac{1}{2 \tan\theta_{\text{st}}}$ , and the  $y$  position of the fitted MMFE8 track evaluated at the average  $z$  position of the trigger stereo hits. The trigger  $y$  measurement is adjusted to account for the slope of the track in the  $x - z$  plane. Calculating the difference of the average trigger  $U$  and  $V$  hits corresponds directly to calculating the difference of the average  $U$  and  $V$  slopes at the NSW, also known as the non-precision slope, which dominates the  $\phi$  measurement.

The  $x$  and  $y$  resolution improves significantly when requiring tighter offline roads, as expected. The RMS of 0.4 mm (29.3 mm) for the  $x$  ( $y$ ) resolution is comparable to what is reported in the TDR. Even with offline roads, however, the distribution seems to reflect two populations of tracks, one sharply peaked at zero and one broadly peaked at zero. The broader distribution is likely caused by  $\delta$ -rays as the muon passes through the chamber. Two event displays of this feature are shown in Figure 10. This motivates using the smallest possible road size at the NSW, for horizontal and stereo planes, to suppress both uncorrelated background hits (e.g. noise) and correlated background hits (e.g.  $\delta$ -rays).

The angular resolution measured with cosmic data is shown in Figure 11. The  $\theta$  resolution is measured as the difference between the slope calculated online by the MMTP FPGA and the slope of the fitted MMFE8 track, after converting each slope to an angle. The online slope is exactly the slope which will be calculated online at the NSW, also known as  $m_X^{\text{local}}$ . The resolution of  $m_X^{\text{local}}$  dominates the res-

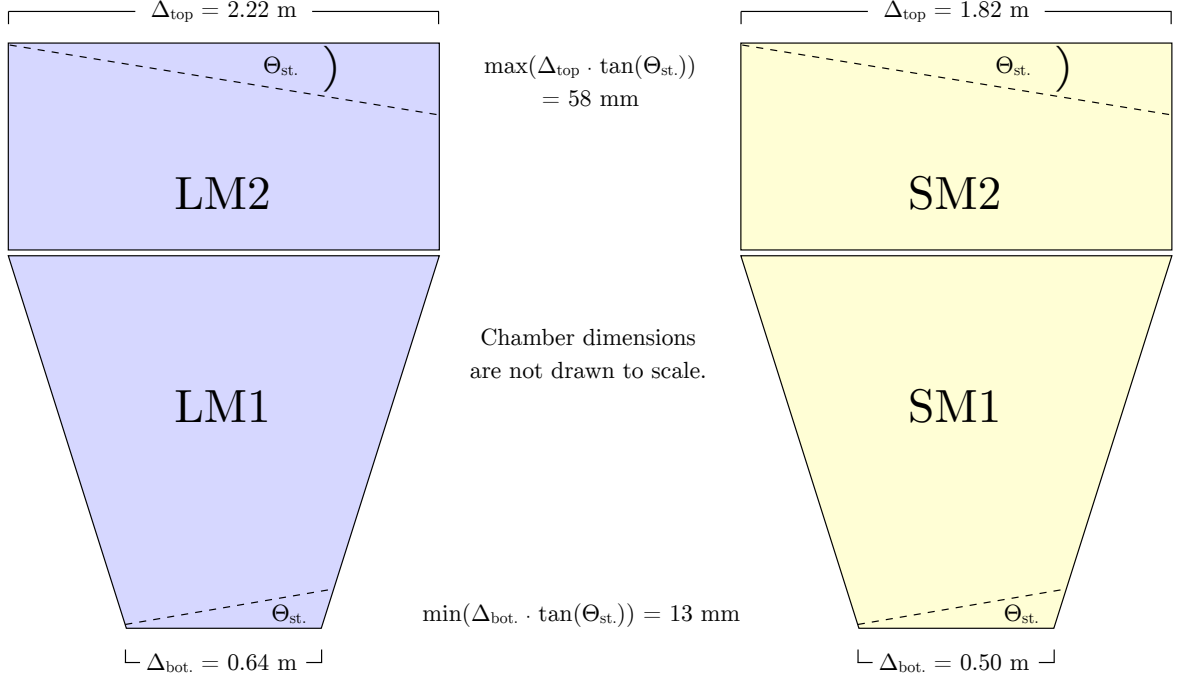


Figure 7: A drawing of the micromegas wedges with the dimensions specified by the NSW. The stereo strips require larger roads than the horizontal strips because they cover between 13 and 58 mm of the detector in the direction of the precision coordinate.

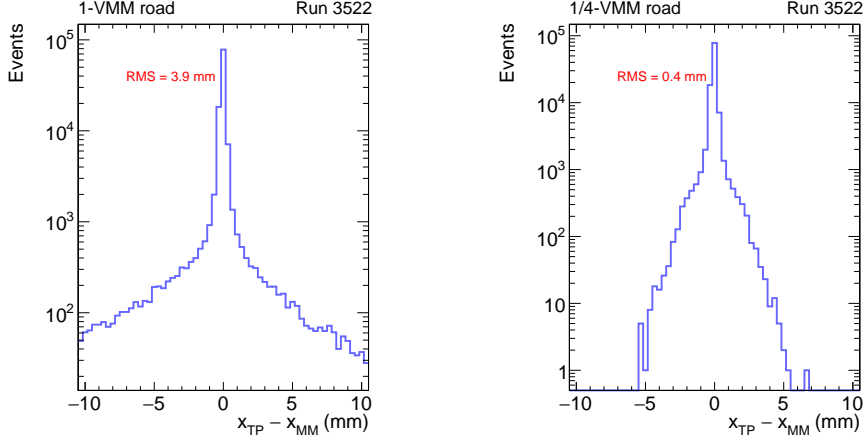


Figure 8: The  $x$  resolution of the MMTP relative to the full readout, using 1-VMM online roads (left) and 1/4-VMM offline roads (right). The tails of the resolution are greatly suppressed with smaller roads.

olution of  $\Delta\theta$ , which measures the consistency of the trigger with the interaction point. The measured  $\theta$  resolution is comparable to what is reported in the TDR, and it improves similarly with smaller road sizes, as expected.

The angular and spatial resolution are shown simultaneously in Figure 12. There is a clear correlation between  $x$  and  $\theta$  in the case of MMTP measurements which disagree significantly with the full MMFE8 readout, since they are equally affected by background hits in the  $X$  planes. In Figure 12 (left), the

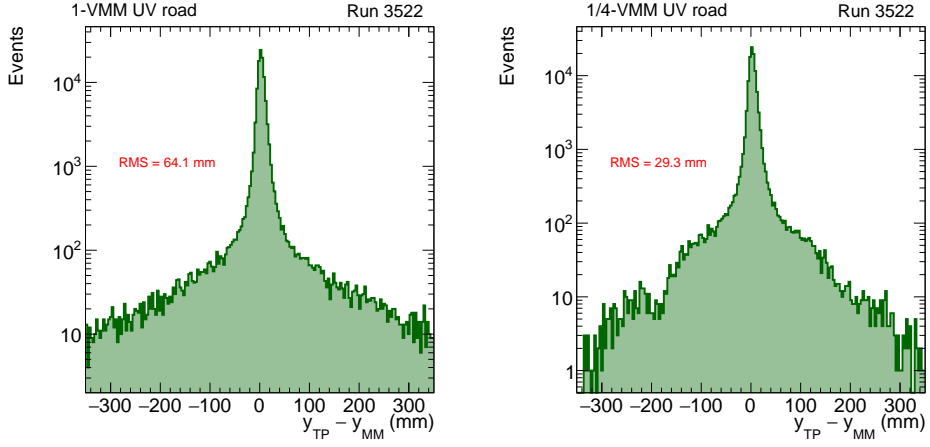


Figure 9: The  $y$  resolution of the MMTP relative to the full readout, using 1-VMM online roads (left) and 1/4-VMM offline roads (right). The tails of the resolution are greatly suppressed with smaller roads.

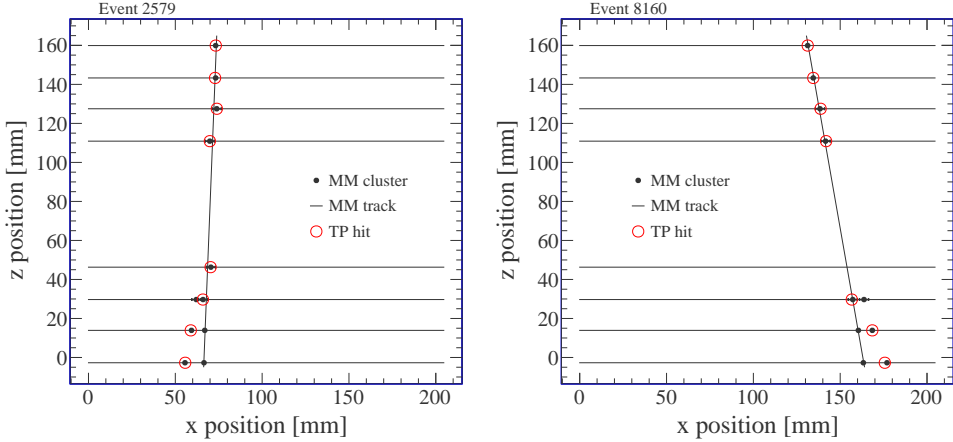


Figure 10: Two event displays likely to include delta rays. The black circles are clusters from the full MMFE8 readout, the black line is the fit to the clusters, and the red circles are the hits chosen by the MMTP. In both cases, the MMTP chooses hits from the delta ray.

long tails are dominated by uncorrelated background hits (noise). In Figure 12 (right), the tails have contributions from uncorrelated (noise) and correlated ( $\delta$ -rays) background hits.

#### 5.4 Time resolution

The time resolution measured with cosmic data is shown in two ways. First, the timing of ART hits within a trigger are compared against themselves. Second, the timing is compared against the scintillator timestamp as a reference.

As discussed in Section 3.2, the MMTP algorithm here collects ART hits in a window of 7 BCs. The measured *BC window* per trigger is then defined as the number of BCs the algorithm actually needed to collect all the hits for a given trigger. For example, if all hits arrive at the same BC, the BC window is 1.

Additionally, the time resolution of individual hits is measured by choosing all possible pairs of hits within a trigger and measuring the difference in their BCIDs. The resolution of this quantity is then related to the time resolution of individual hits by  $\sigma(t_i - t_j) = \sqrt{2} \sigma(t)$ .

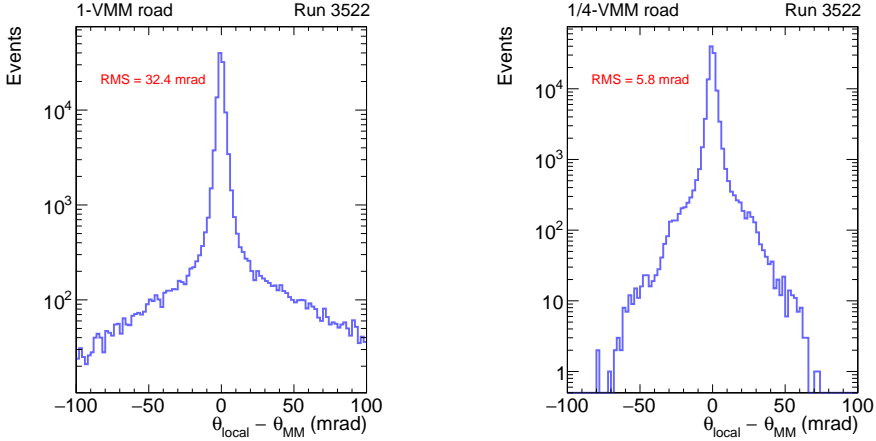


Figure 11: The  $\theta$  resolution of the MMTP relative to the full readout, using 1-VMM online roads (left) and 1/4-VMM offline roads (right). The tails of the resolution are greatly suppressed with smaller roads.

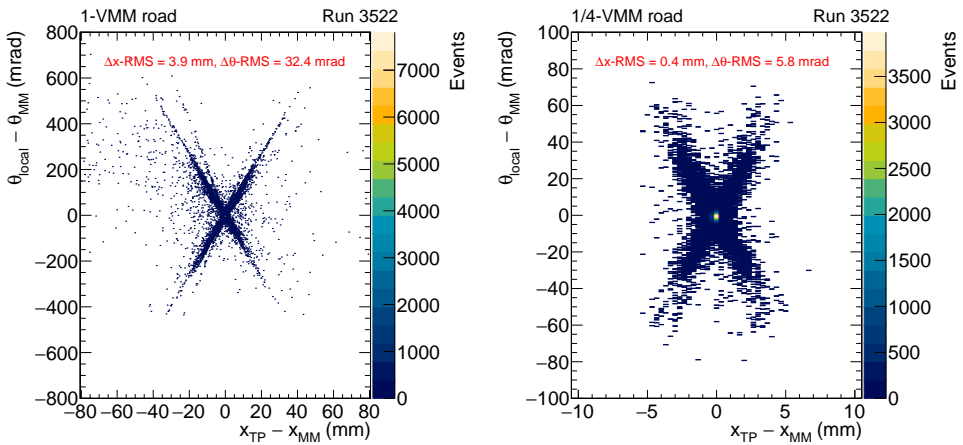


Figure 12: The  $x$  and  $\theta$  resolution of the MMTP relative to the full readout, using 1-VMM online roads (left) and 1/4-VMM offline roads (right). The tails of the resolution are greatly suppressed with smaller roads.

These distributions are shown in Figure 13. The measured time resolution is worse than what is reported in the TDR. Simulation of the micromegas in the NSW have suggested a BC window of 2 BCs would be sufficient to collect trigger hits with better than 99% efficiency [6]. The measurements here indicate a window of 5-10 BCs is more likely needed to achieve a good efficiency. The distribution of  $\Delta BC$  for pairs of ART hits gives a fitted  $\sigma$  of 2.15 BCs, corresponding to a time resolution of 38 ns per hit.

A global time measurement per trigger is also of interest for the NSW. This is needed to match tracks found in the NSW with tracks found by the TGCs in the big wheel, and it will be one of the parameters sent to downstream clients of the NSW trigger, along with the position and quality of a trigger.

A per-trigger time resolution is measured with cosmic data by comparing the time of hits within the trigger to the time reported by the scintillator, which has a resolution of 1-2 ns after being processed by the MMTP FPGA. Two methods are considered for making a trigger-level BCID: the average BCID of all hits, and the earliest BCID of all hits. The distributions are shown in Figure 14. The average BCID

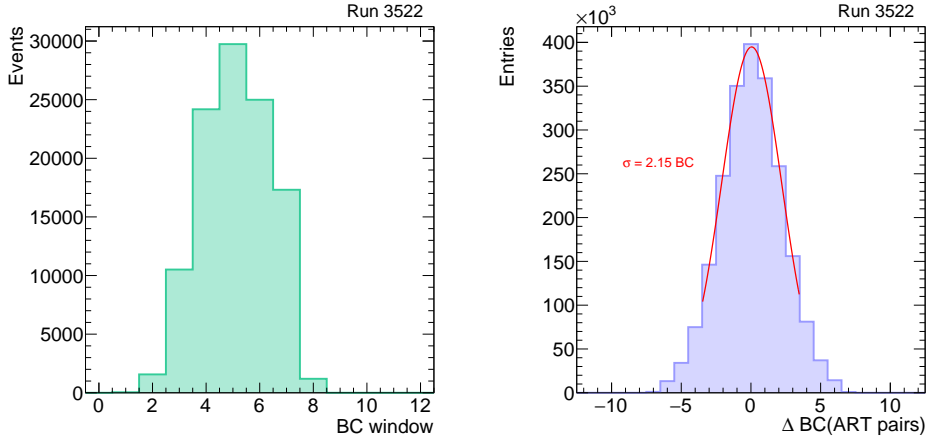


Figure 13: The time window required to record all hits in a trigger (left) and the  $\Delta\text{BC}$  of all pairs of hits in a trigger (right). A gaussian fit is overlaid on the distribution of  $\Delta\text{BC}$  and describes the data well.

agrees with the reference BCID with  $\sim 50\%$  efficiency, and the earliest BCID agrees with reference with  $\sim 41\%$  efficiency.

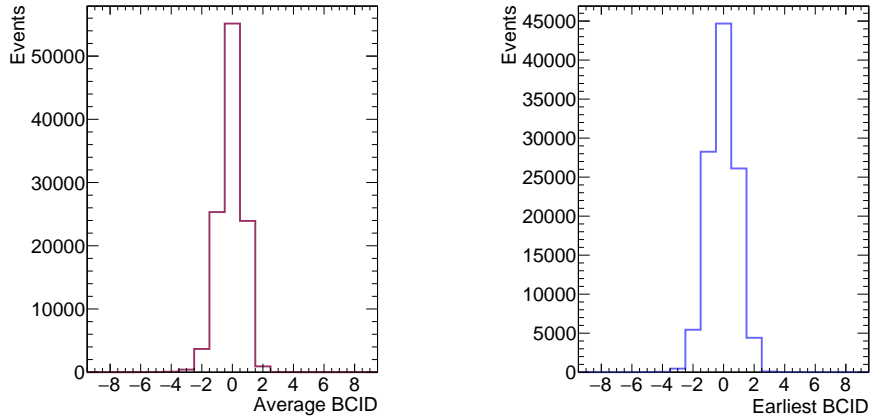


Figure 14: The time resolution of the MMTP relative to the scintillator. The BCID of the trigger can be defined as the average BCID of the ART hits (left) or the earliest BCID (right). Choosing the average BCID performs better than choosing the earliest.

## 5.5 Integration time

The performance of the MMTP is also considered for different integration times of the front-end VMM2 chip. The integration times considered are 200 ns, 100 ns, and 50 ns. The results presented elsewhere in the section are exclusively with 200 ns integration time.

The efficiency, spatial resolution, and angular resolution are found to not depend significantly on the integration time. They are shown in Appendix ???. The time resolution of ART hits and the trigger improve with smaller integration time, as shown in Figures 15, 16, 17, and 18. Specifically, the time resolution of individual hits decreases from 40 ns to 32 ns when shortening the integration time from 200 ns to 50 ns.

Operating the NSW with short integration then presents one option for improving the time resolution of the micromegas trigger. However, we note the micromegas detectors used in this note were operated with a high voltage of 560-570 V, near the maximum voltage. At lower voltage, the efficiency loss of shorter integration time would become a more significant factor.

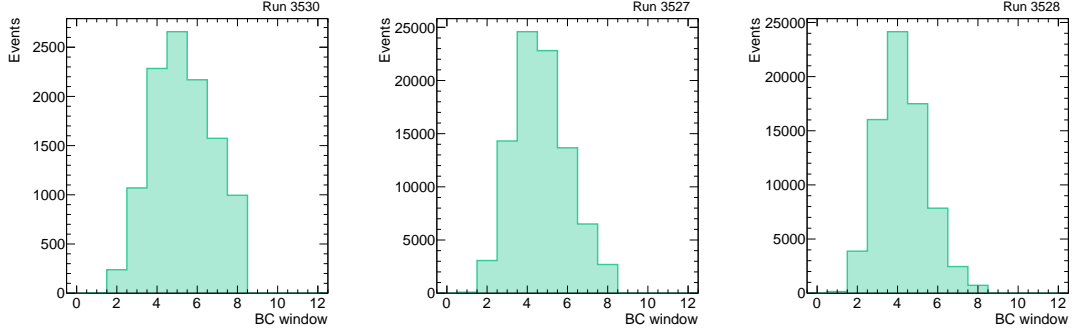


Figure 15: The time window required to record all hits in a trigger for data collected with 200 ns (left), 100 ns (middle), and 50 ns (right) integration time in the VMM. The window decreases as the integration time decreases.

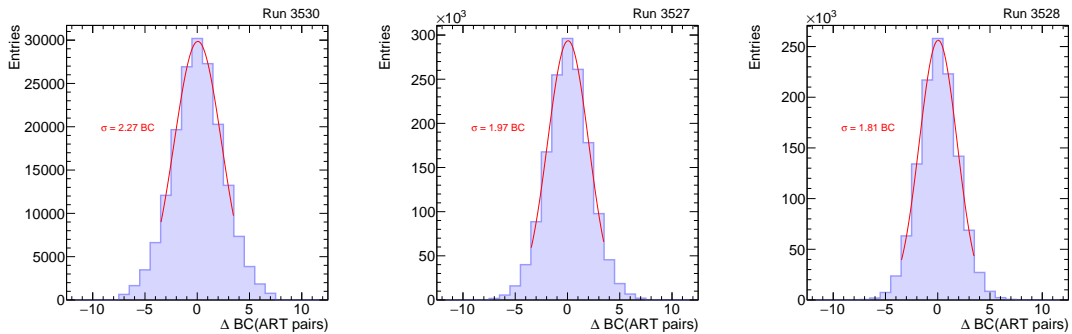


Figure 16: The  $\Delta BC$  of all pairs of hits in a trigger for data collected with 200 ns (left), 100 ns (middle), and 50 ns (right) integration time in the VMM. The distribution is narrower as the integration time decreases.

## 6 Conclusion

The performance of the micromegas Address in Real Time (ART) and trigger processor is shown. The performance is measured with hundreds of thousands of cosmic muons recorded at the Harvard cosmic ray test stand, which employs a full trigger electronics path with prototype hardware: MMFE8s equipped with VMM2, the FPGA-based ADDC V1, and a micromegas trigger processor (MMTP) implemented on a VC707 FPGA evaluation board.

Given a track identified by the full front-end MMFE8 readout, the efficiency of the micromegas trigger is  $> 99\%$ . The spatial, angular, and time resolution of the MMTP is measured with the front-end readout as reference, and the spatial and angular resolutions are found to be comparable to predictions made in the TDR. The time resolution is worse than predicted. The time resolution improves with shorter integration time; however, even with the shortest integration time considered, the time resolution is worse than anticipated.

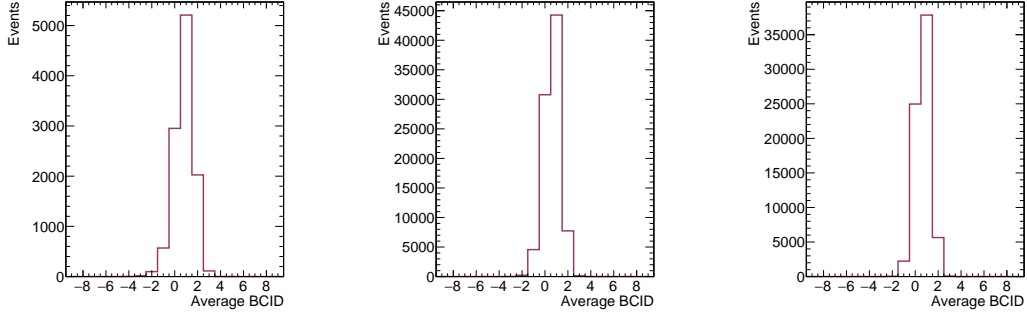


Figure 17: The time resolution of the MMTP relative to the scintillator, where the BC of the trigger is defined as the average BCID of the ART hits, for data collected with 200 ns (left), 100 ns (middle), and 50 ns (right) integration time in the VMM.

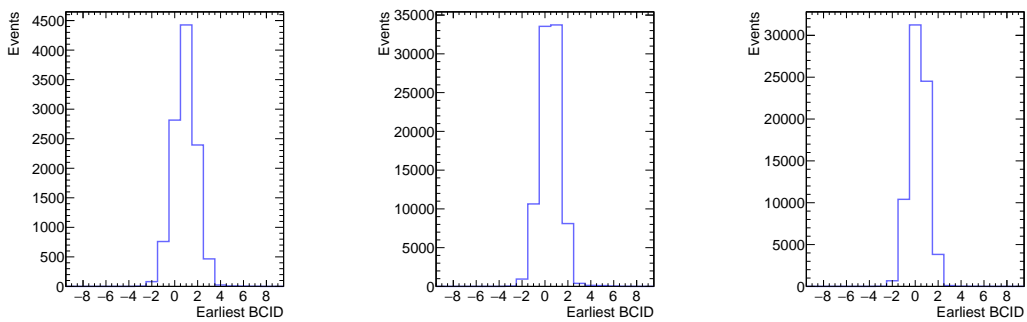


Figure 18: The time resolution of the MMTP relative to the scintillator, where the BC of the trigger is defined as the earliest BCID of the ART hits, for data collected with 200 ns (left), 100 ns (middle), and 50 ns (right) integration time in the VMM.

## References

- [1] ATLAS New Small Wheel Technical Design Report. [ATLAS-TDR-020](#).
- [2] B. Clark et. al. An Algorithm for Micromegas Segment Reconstruction in the Level-1 Trigger of the New Small Wheel. [ATL-COM-UPGRADE-2014-012](#).
- [3] S. Chan et. al. Micromegas Trigger Processor Algorithm Performance in Nominal, Misaligned, and Misalignment Corrected Conditions. [ATL-COM-UPGRADE-2015-033](#).
- [4] P. Giromini et. al. Performance of a Micromegas octuplet in the time of MMFE8 noise. [ATL-COM-MUON-2017-036](#).
- [5] P. Giromini et. al. Performance of a Micromegs octuplet after removing the major cause of noise. [ATL-COM-MUON-2017-040](#).
- [6] Simulation of the ATLAS New Small Wheel (NSW) System. [ATL-MUON-SLIDE-2017-248](#).